Kinetic Interpretation of a Negative Time Constant Impedance of Glucose Electrooxidation

I. Danaee,[†] M. Jafarian,*[,†] F. Forouzandeh,[†] F. Gobal,[‡] and M. G. Mahjani[†]

Department of Chemistry, K. N. Toosi University of Technology, P.O. Box 15875-4416 Tehran, Iran, and Department of Chemistry, Sharif University of Technology, P.O. Box 11365-9516, Tehran, Iran

Received: August 3, 2008; Revised Manuscript Received: September 30, 2008

Nickel−copper alloy modified glassy carbon electrodes (GC/NiCu) prepared by galvanostatic deposition were used for the electrocatalytic oxidation of glucose in alkaline solutions. The electro-oxidation of glucose in a 1 M NaOH solution at different concentration of glucose was studied by the method of ac-impedance spectroscopy. The impedance behavior show different patterns, capacitive, and inductive loops and negative resistances, at different applied anodic potential. The influence of the electrode potential on the impedance pattern is studied and a quantitative explanation for the impedance behavior of glucose oxidation is put forward by a proposed mathematical model. At potentials higher than 0.5 V/Ag−AgCl, a pseudoinductive behavior is observed while at higher than 0.53 V/Ag−AgCl, impedance pattern is reversed to the second, third, and forth quadrants. The conditions required for the reversing of impedance pattern are delineated with the use of the impedance model. The previously proposed electrooxidation mechanism for glucose on GC/NiCu electrode was found to reproduce the experimental impedance plots.

1. Introduction

Electrocatalytic processes involving the oxidation of sugars are of great interest in many areas, ranging from medical applications to wastewater treatment and from the construction of biological fuel cells to analytical applications in the food industry.[1−4]

The investigation of glucose electrochemical oxidation began in the 1960s and has remained a very active research area.[5,6] Bagotzky and Vassilyev[7] first reported the electrooxidation of glucose in an acidic medium. At about the same time Bockris et al.[8] studied this reaction at high temperature in alkaline solutions.

Oxidizable transition metal electrodes[9−14] provide simple routes for the catalytic oxidation of carbohydrates at constant applied potentials. Fleischmann studied Ni electrodes and explained the oxidation of alcohols and amines on the basis of a mechanism involving electron-transfer mediation by a $Ni(OH)_2$/NiOOH redox couple at the anodized electrode surface.[15] A similar mechanism has been suggested by Luo et al. to explain the anodic oxidation of glucose on Ni electrodes in alkaline media.[16] Pure Cu electrodes have demonstrated activity for the anodic oxidation of carbohydrates in alkaline media. However, the corresponding response mechanism remains somewhat controversial. Nevertheless, following the evidence for Ni electrodes, it has been suggested that a Cu(II)/Cu(III) redox couple at the surface of the anodized Cu electrodes works through an electron-transfer mediated mechanism for carbohydrate oxidation.[17,18]

The study of alloy electrodes are motivated primarily from the anticipation of a synergistic electrocatalytic benefit from the combined properties of the components of alloys. Furthermore, the use of preanodized alloy electrodes is expected to offer the advantage of ease of preparation and long-term stability in comparison with thermally prepared and electrolytically deposited mixed-oxide film electrodes. Kuwana and co-workers investigate the alloy electrodes in carbohydrate oxidation on Ni-based alloys containing high percentages of Cu and Cr.[19,20] One promising characteristic of such alloy electrodes is the resistance to corrosion in alkaline media.

Electrochemical impedance spectroscopy (EIS) is a good tool to analyze the kinetics of electrode reactions. The advantage of EIS over DC techniques is that this steady-state technique is capable of probing relaxation phenomena over a wide frequency range. The measured impedance can be presented in the form of imaginary vs real parts at various measurement frequencies, Nyquist plots, which appear as a multitude of semicircles and lines.[21−24] Equivalent electrical circuits capable of generating the same impedance plots in response to a potential stimuli are used for the interpretations that associate kinetics and transport properties with the circuit elements. Often, discrepancies and ambiguities hamper the analysis.[22] Many equivalent circuits can show the same impedance characteristics and supplementary data and chemical intuition help to select the most relevant one. Also, it may be difficult to find electrochemical equivalent to some electrical circuit elements and vice versa.[23−26] Inductive loops are often difficult to account for and are related to desorptive generation of sites for the charge transfer processes of electroactive constituents.[25−28]

There has been a recent resurgence of interest in the studies of the negative impedance behavior in electrochemical systems like electrocatalysis, electrodeposition and electrodisolution.[29,30] Although the mechanistic origin of the negative impedance is quite different for various systems (desorption from a catalyst, adsorption of an inhibitor, double layer repulsion), they are all described by essentially the same mathematical model whose properties are clearly insensitive to the precise chemical origin of the negative $dI_F(E)/dE$ with E and I_F are the applied potential and Faradaic current.

The purpose of this work is the analysis of reaction mechanism of the electrooxidation of glucose on NiCu modified glassy carbon in NaOH solution at different glucose concentration and oxidizing potentials by impedance spectroscopy

* Corresponding author. E-mail address: mjafarian@kntu.ac.ir. Tel.: (009821) 22853551. Fax: (009821) 22853650.
[†] K. N. Toosi University of Technology.
[‡] Sharif University of Technology.

10.1021/jp8069173 CCC: $40.75
Published on Web 11/14/2008

dominated by negative time constants. The analysis of the theoretical impedance function provides important information on the kinetic parameters.

2. Methods and Materials

Sodium hydroxide, nickel sulfate, sodium citrate, and glucose used in this work were Merck products of analytical grade and were used without further purifications. Doubly distilled water was used throughout. Electrochemical studies were carried out in a conventional three electrode cell powered by an electrochemical system comprising of EG&G model 273 potentiostat/galvanostat and Solartron model 1255 frequency response analyzer. The system is run by a PC through M270 and M389 commercial softwares via a GPIB interface. The frequency range of 100 kHz to 15 mHz and the modulation amplitude of 5 mV were employed for impedance measurements. Fitting of experimental impedance measurements to the proposed equivalent circuit was done by means of home written least-squares software based on the Marquardt method for the optimization of functions and Macdonald weighting for the real and imaginary parts of the impedance.[31,32] A dual Ag/AgCl−saturated KCl, a Pt wire, and a glassy carbon (GC) disk electrode were used as the reference, counter, and working electrodes respectively. All studies were carried out at 298 ± 2 K.

The GC disk electrode supplied by EG&G was further polished with 0.05 μm alumina powder on a polishing microcloth and rinsed thoroughly with doubly distilled water prior to modification. Films of nickel were formed on the GC surface by galvanostatic deposition from a solution composed of 0.7 M $NiSO_4$ + 0.2 M Na_3citrate at the current density of 10 mA cm^{-2} and for 300 s. Working electrode was placed in the middle of the cell and electrolyte was stirred with magnetic stirrer during electrodeposition. The chemical composition of the deposit was evaluated by scanning electron microscopy (SEM, Philips XL30) equipped with the energy dispersive X-ray (EDX).

3. Results and Discussion

Figure 1a shows the consecutive cyclic voltammograms (CV) of a nickel−copper alloy electrode in 1 M NaOH solution recorded at a potential sweep rate of 100 mV s^{-1}. The result of chemical composition analysis obtained by EDX revealed that the composite contains 79% Ni and 21% Cu, the compositions are in weight percents, Figure 1b. In the first sweep, Figure 1a, a pair of redox peaks appear at 560 and 430 mV/Ag−AgCl that are assigned to the Ni^{2+}/ Ni^{3+} redox couple according to

$$Ni(OH)_2 + OH^- \leftrightarrows NiOOH + H_2O + e^- \qquad (1)$$

In the subsequent cycles both the anodic and cathodic peaks shift negatively and stabilize pointing to higher energies (potential) required for nucleation of NiOOH in the first cycle. The enhanced baseline current of the first cycle is associated with the oxidation of Ni to Ni^{2+} with the subsequent formation of α-$Ni(OH)_2$ film with slow concomitant conversion to β-$Ni(OH)_2$. The current growth with the number of potential scans indicates the progressive enrichment of the accessible electroactive species Ni^{2+} and Ni^{3+}on or near the surface. After prolonged cycling, the redox peak potential are stabilized at 500 and 385 mV/Ag−AgCl.

Initially a $Ni(OH)_2$ layer is formed on the surface of NiCu alloy during the positive potential scan.[33] The rapid formation of $Ni(OH)_2$ at low potential leads to a Cu-rich metal surface which is oxidized to Cu_2O later and further to $Cu(OH)_2$ at longer times.[33] Therefore, the surface layer is subsequently transformed to a mixture of NiOOH and $Cu(OH)_2$.[33] Also, some $Cu(OH)_2$ and CuO can be oxidized further to Cu^{3+} oxide prior to evolution of oxygen.[17] In consecutive cyclic voltammograms of nickel−copper alloy the peak potentials except the first cycle are invariable, suggesting that the phase transformation of Ni oxyhydroxide from β to γ is inhibited. It is reported that there are four phases produced over the lifetime of a nickel hydroxide electrode, β-$Ni(OH)_2$, α-$Ni(OH)_2$, β-NiOOH, and γ-NiOOH.[34,35] The well-known Bode diagram identifies the phase transformations that are likely to occur during a normal cycle. β-$Ni(OH)_2$ is first oxidized into β-NiOOH and the subsequent reduction during the cell discharge can be considered as the intercalation into the β phase of one proton and one electron per Ni atom. Alternatively, γ-NiOOH is reduced into hydrated α-$Ni(OH)_2$ phase, which is unstable in strong alkali and ages to the β-form. In addition, β-NiOOH is partially converted to γ-NiOOH under experimental conditions of overcharge, high charge/discharge rates and high alkali concentrations.[36,37] However, these physical transformations occur slowly and are generally incomplete so that α/γ and β/β systems coexist under steady state conditions.[37] It is well-known that the formation of γ-NiOOH phase is associated with swelling or volume expansion of nickel film electrodes with subsequent microcracks and disintegration of the nickel oxide film.[36,37] Lower interelectrode spacing results in lower internal resistance and therefore better efficiencies of the electrode processes.[36,37] Therefore, β-NiOOH phase is expected to be an electroactive material for high electrochemical performance in alkaline solution. Thus, addition of copper hydroxide to the nickel oxyhydroxide species represents a very efficient strategy of suppressing formation of γ-NiOOH phase. Similar electrochemical behavior was observed for alloys obtained by addition of several percent of Cd, Zn, Co, Ca, Ti, and other elements as solid solutions to the nickel hydroxide.[36,38,39]

Figure 2 shows cyclic voltammograms of GC/NiCu electrode in 1 M NaOH solution in the absence (1) and presence (2) of glucose (9 mM) and at a potential sweep rate of 10 mV s^{-1}. On GC/NiCu electrode, oxidation of glucose appeared as a typical electrocatalytic response. The anodic current increased with respect to that observed for the modified surface in the absence of glucose and it was followed by decreasing the cathodic current in the presence of glucose in solution. Moreover, in the presence of glucose, the onset of the oxidation potential of the Ni(II) moiety shifted to positive value and enhanced upon increasing the concentration of glucose. This indicates a strong interaction of glucose with the surface already covered by low valance nickel species.

The decreased cathodic current that ensued the oxidation process in the reverse cycle indicated that the rate determining step certainly involves glucose and that it was incapable of reducing the entire high valent nickel species formed in the oxidation cycle. The electrocatalytic oxidation of glucose occurs not only in the anodic but also continues in the initial stage of the cathodic half-cycle. Glucose molecules adsorbed on the surface are oxidized at higher potentials parallel to the oxidation of Ni^{2+} to Ni^{3+} species. The later process has the consequence of decreasing the number of sites for glucose adsorption that along with the poisoning effect of the products or intermediates of the reaction tends to decrease the overall rate of glucose oxidation. Thus, the anodic current passes through a maximum as the potential is anodically swept. In the reverse half-cycle, the oxidation continues and its corresponding current goes through a maximum due to the regeneration of active sites for the adsorption of glucose as a result of the removal of adsorbed

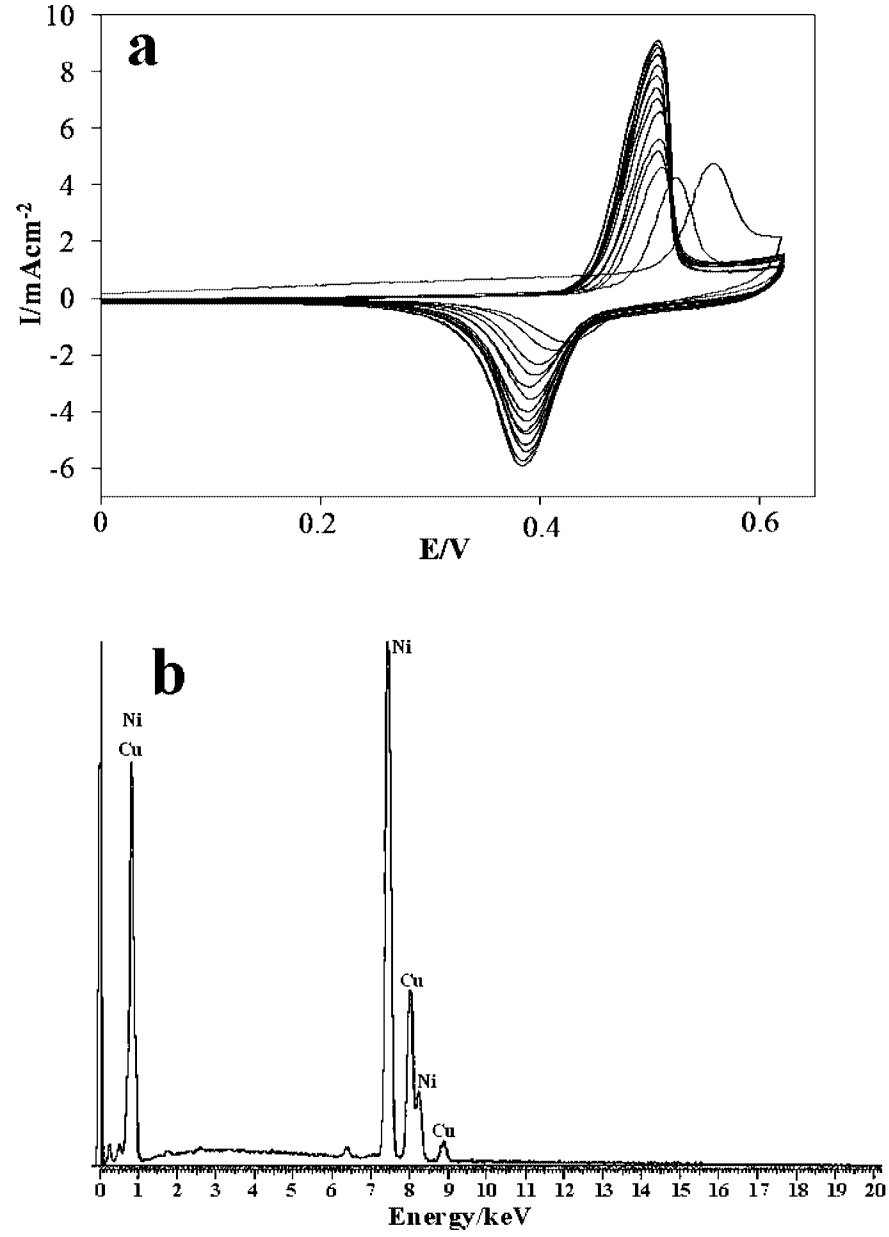

Figure 1. (a) Consecutive cyclic voltammogram of GC/NiCu oxidation in 1 M NaOH comprised of different sweep numbers (1, 2, 3, 4, 5, 10, 15, 20, 25, 30, 35, 40, 45, and 50) at a scan rate of 100 mV s^{-1}. (b) EDX results of the chemical composition of the surface of NiCu alloy.

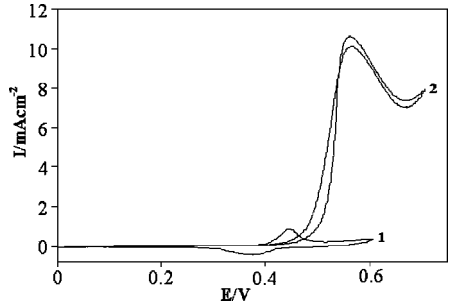

Figure 2. Cyclic voltammograms in the absence (1) and the presence of 9 mM of glucose (2) on GC/NiCu electrode in 1 M NaOH solution. The potential sweep rate was 10 m Vs^{-1}.

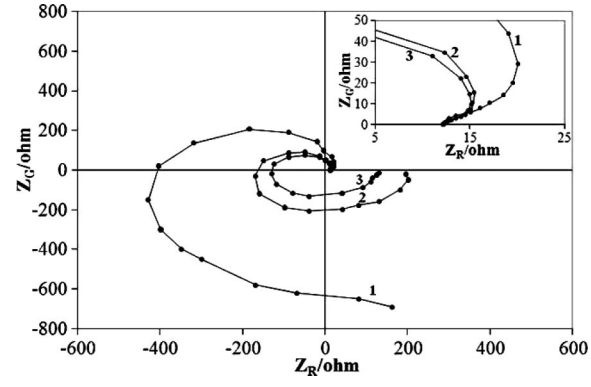

Figure 3. Nyquist diagrams of GC/NiCu electrode in different concentration of glucose in 1 M NaOH: (1) 7, (2) 9, and (3) 11 mM. DC potential is 0.55 V/Ag−AgCl.

intermediates and products. Surely, the rate of glucose oxidation as signified by the anodic current in the cathodic half-cycle drops as the unfavorable cathodic potentials are approached.

Figure 3 shows the Nyquist diagrams of GC/NiCu electrode recorded at the oxidation peak potential for glucose concentrations in the range of 7−11 mM. The Nyquist diagrams consist of three slightly depressed overlapping semicircles in high, medium and low frequency. The depressed semicircle in high

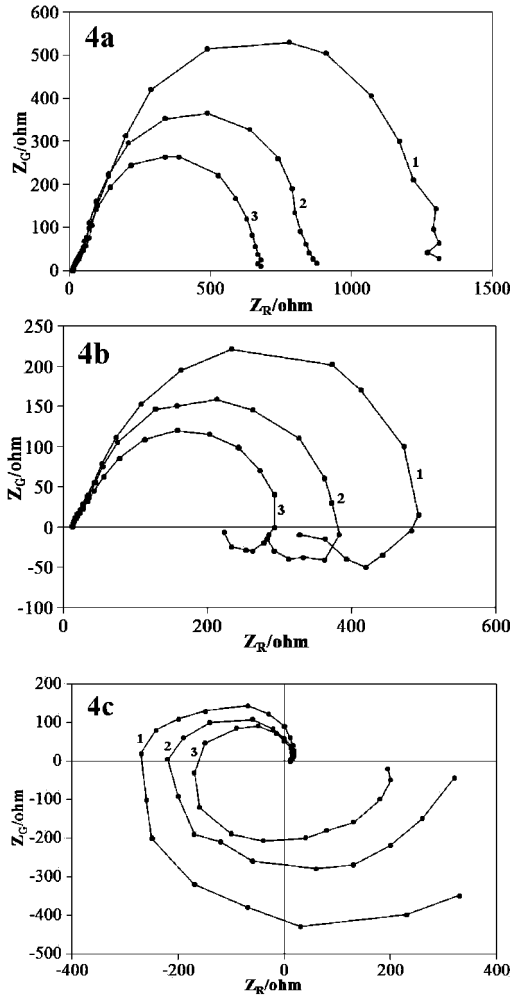

Figure 4. Experimental Nyquist diagrams as a function of applied potential for glucose electrooxidation on GC/NiCu electrode in 9 mM glucose: (a) at potentials (1) 0.47, (2) 0.48, and (3) 0.49 V vs Ag−AgCl; (b) at potentials (1) 0.5, (2) 0.51, and (3) 0.52 V vs Ag−AgCl; (c) at potentials (1) 0.53, (2) 0.54, and (3) 0.55 V vs Ag−AgCl.

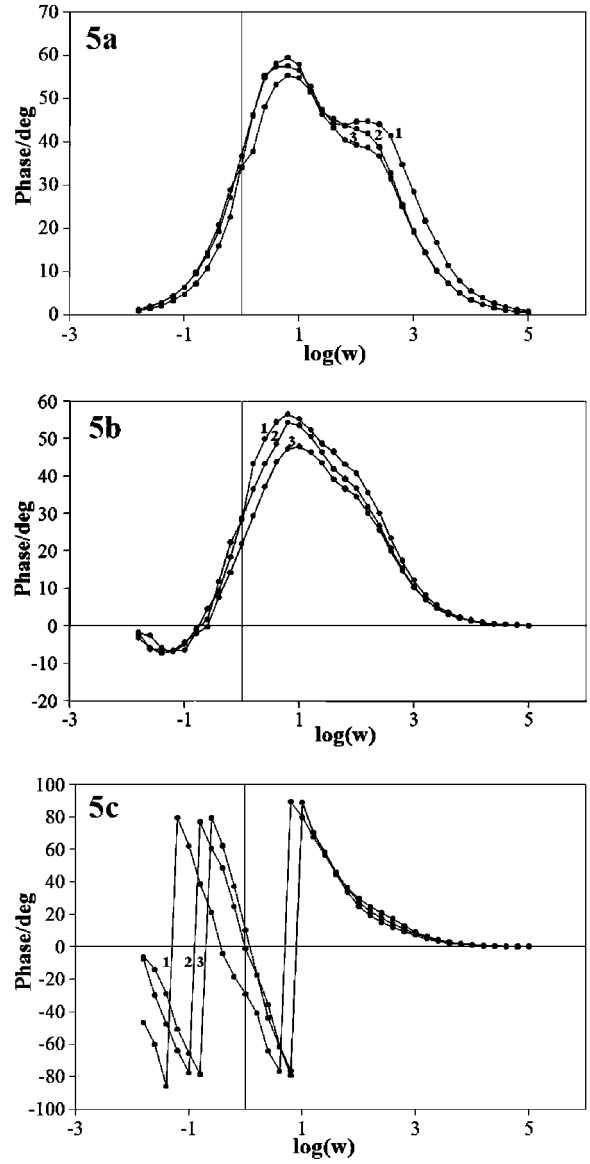

Figure 5. Experimental phase shift plots as a function of applied potential for glucose electrooxidation on GC/NiCu electrode in 9 mM glucose: (a) at potentials (1) 0.47, (2) 0.48, and (3) 0.49 V vs Ag−AgCl; (b) at potentials (1) 0.5, (2) 0.51, and (3) 0.52 V vs Ag−AgCl; (c) at potentials (1) 0.53, (2) 0.54, and (3) 0.55 V vs Ag−AgCl.

frequency region can be related to the combination of charge transfer resistance and the double layer capacitance. It is observed that the charge transfer characteristic appear in the first quadrant, two loops in medium and low frequencies are located in the second, third, and forth quadrants.

Figure 4 shows Nyquist plots of the impedance of glucose electrooxidation at different potentials in 9 mM glucose. At 0.48 V/Ag−AgCl, two large depressed capacitive semicircle are observed, Figure 4a, revealing a slow reaction rate of glucose oxidation. The semicircles in the high frequency side is due to charge transfer and the one at the low frequency end is due to the adsorption of the intermediates. Bode phase plots are shown in Figure 5a where two well resolved peaks are observed pointing to two depressed and overlapping semicircles in Nyquist plot. The equivalent circuit compatible with the Nyquist diagram is depicted in Figure 6a. To obtain a satisfactory impedance simulation of glucose electrooxidation, it is necessary to replace the capacitor, C with a constant phase element (CPE) Q in the equivalent circuit. The most widely accepted explanation for the presence of CPE behavior and depressed semicircles on solid electrodes is microscopic roughness, causing an inhomogeneous distribution in the solution resistance as well as in the double-layer capacitance.[40] In this electrical equivalent circuit, R_s, CPE_{dl}, and R_{ct} represent solution resistance, a constant phase element corresponding to the double layer capacitance, and the charge transfer resistance. CPE_{ads} and R_{ads} are the electrical elements related to the adsorption of reaction intermediates. In this circuit the charge transfer resistance of the electrode reaction is the circuit element that has a simple physical meaning describing how fast the rate of charge transfer during glucose electrooxidation changes with changing electrode potential when the surface coverage of the intermediate is held constant.

To corroborate equivalent circuit the experimental data are fitted to equivalent circuit and the magnitudes of the circuit elements are obtained. Table 1 illustrates the equivalent circuit parameters derived from the impedance spectra of glucose oxidation.

In the potential range of 0.5−0.52 V, a pseudoinductive behavior was observed, Figure 4b, where the large semicircles at high and medium frequencies are terminated to a small arc in the forth quadrant at low frequency and with all the diameters decreasing sharply with increasing potential. This inductive behavior is due to the relaxation phenomenon characteristics

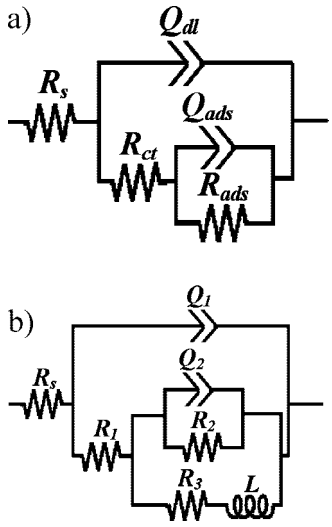

Figure 6. (a) Equivalent circuits compatible with the experimental impedance data presented in Figure 4a. (b) Equivalent circuits compatible with the experimental impedance data presented in Figure 4b and c for glucose electrooxidation on the GC/NiCu electrode.

of the generation of further active sites upon the desorption of the intermediates[24,25] and further adsorption of electroactive constituents, glucose, on active sites.[25] Negative phase angle also is observed in the corresponding bode phase shift, Figure 5b. As potential arrives at 0.53 V/Ag−AgCl, a change in the shape of impedance plots happens where the two loops in the medium and low frequencies reversing to the second, third and forth quadrants presumably due to the passivation of electrode surface[23,24] as shown in Figure 4c. The phase sift, Figure 5c, of experimental impedance data shows an abrupt jump between the positive and negative values of phase angle, indicating the change of the rate determining step of elecrooxidation of glucose on GC/NiCu in potential range 0.47−0.55 V.

The equivalent circuit compatible with the Nyquist diagram recorded in potential range of 0.5−0.55 V is depicted in Figure 6b. Table 1 illustrates the equivalent circuit parameters for the impedance spectra of glucose oxidation in different applied potential. As previously mentioned the first depressed semicircle in the entire potential range is due to charge transfer resistance and the inductive behavior appearing in higher potentials is due to the regeneration of active sites for the adsorption of glucose.

The EIS results indicate that the glucose electrooxidation on GC/NiCu catalyst at various potentials shows different impedance behaviors. In attempt to clarify the oxidation of alcohols at the nickel electrode covered by nickel hydroxide in alkaline solution where different mechanisms have been proposed in the literature is considered. In the oxidation of alcohols in 1 M KOH on nickel electrode covered by nickel hydroxide, Fleischmann et al.[15,41] proposed a mechanism of alcohol oxidation and suggested that the NiOOH acts as an electrocatalyst. This was mainly based on the experimental observation that in the course of a cyclic voltammogram alcohols and other organic compounds are oxidized at a potential which coincided exactly with that where NiOOH was formed, and on the disappearance of the NiOOH reduction peak in the negative half-cycle. However, the role of NiOOH as an electrocatalyst has been questioned by some authors.[42,43] Others[44] reported that methanol oxidation takes place after the complete oxidation of $Ni(OH)_2$ to NiOOH. El-Shafei[45] studied the oxidation of methanol on the nickel hydroxide/glassy carbon modified electrode in alkaline medium and found that methanol oxidation occurred via Ni^{3+} species (mainly NiOOH). On the other hand, Taraszewska and Roslonek[44] proposed that methanol molecules penetrate the nickel hydroxide film and are oxidized by the OH^- ions trapped in the film. Vertes and Horanyi[43] while criticizing the above mechanism raised doubts on the role of NiOOH as electrocatalyst. Their proposition is based on their own experimental observation in the case of oxidation of alcohols on Ni in 1 M NaOH. In their case a new oxidation peak for the alcohol was obtained at a potential much more positive of the oxidation of $Ni(OH)_2$, whereas the redox peaks due to $Ni(OH)_2 \leftrightarrow$ NiOOH conversion remained unaffected. These observations are contrary to those of Fleischmann et al. who observed the electrocatalysis at the same potential that of $Ni(OH)_2$ conversion.

On account of the high anodic currents in the presence of glucose we tend to assume that part of the current is due to the elecrocatalysis phenomenon while partly is due to the direct electrodic oxidation of glucose on the surface (probably NiOOH part). The redox transition of nickel species present in the film is

$$\mathrm{Ni(II)} \xleftrightarrow{k_1,\,k_{-1}} \mathrm{Ni(III)} + \mathrm{e}^- \tag{2}$$

and glucose is oxidized on the modified surface via the following reaction:

$$\mathrm{Ni}^{3+} + \text{glucose} \xrightarrow{k_2} \mathrm{Ni}^{2+} + \text{intermediate} \tag{3}$$

$$\mathit{N}\mathrm{i}^{3+} + \text{intermediate} \xrightarrow{k_3} \mathrm{Ni}^{2+} + \text{products} \tag{4}$$

$$\mathrm{Ni}^{3+} - \text{glucose} \xrightarrow{k_4} \mathrm{Ni}^{3+} - \text{intermediate} + \mathrm{e} \tag{5}$$

$$\mathrm{Ni}^{3+} - \text{intermediate} \xrightarrow{k_5} \mathrm{Ni}^{3+} - \text{products} + \mathrm{e} \tag{6}$$

Equations 3 and 4 are according to Fleischmann mechanism, while in eqs 5 and 6, Ni^{3+} is used as active surface for glucose oxidation. Observation of a high current density in presence of glucose in comparison to the $Ni(OH)_2$ is in accord with eqs 5 and 6. Gluconolactone[46] as well as formats and oxalates[34] have been reported as the oxidation products.

On the basis of the above mechanism, the kinetics of the oxidation reaction can be expressed as

$$v_1 = 2k_1^{\mathrm{o}}(1 - \theta_{\mathrm{Ni^{3+}}}) \exp\left(\frac{E}{b_1}\right) - 2k_{-1}^{\mathrm{o}}\theta_{\mathrm{Ni^{3+}}} \exp\left(-\frac{E}{b_{-1}}\right) \tag{7}$$

$$v_2 = k_2^o C_g (1 - \theta_i)\theta_{Ni^{3+}} \quad (8)$$

$$v_3 = k_3^o \theta_i \theta_{Ni^{3+}} \quad (9)$$

$$v_4 = k_4^o C_g \theta_{Ni^{3+}} (1 - \theta_i) \exp\left(\frac{E}{b_2}\right) \quad (10)$$

$$v_5 = k_5^o \theta_i \theta_{Ni^{3+}} \exp\left(\frac{E}{b_3}\right) \quad (11)$$

where k_i ($i = 1, -1, 2, 3, 4, 5$) are rate constants, b_i ($i = 1, -1, 2, 3$) are the Tafel slope, $\theta_{Ni^{3+}}$ is the fractional coverage of Ni^{3+}, θ_i is the surface coverage of reaction intermediates, C_g is the glucose concentration, and v_i is the reaction rate. On the basis of the proposed mechanism, the Faradaic current density (I_F) can be written as

$$I_F = (v_1 + v_4 + v_5)F \quad (12)$$

In the steady state, the Faradaic current density (I_F) of glucose electrooxidation can be expressed as a function of electrode potential and two state variable, fractional coverage of Ni^{3+} ($\theta_{Ni^{3+}}$) and the surface coverage of reaction intermediates (θ_i).

$$I_F = f(E, \theta_{Ni^{3+}}, \theta_i) \quad (13)$$

If a sufficiently small perturbation signal $\Delta E = |\Delta E| \exp(jwt)$ is applied to the electrode, the deviation of I_F from the steady state can be approximated by the first order of the Tailor's series expansion:

$$\Delta I_F = \left(\frac{\partial I_F}{\partial E}\right)\Delta E + \left(\frac{\partial I_F}{\partial \theta_{Ni^{3+}}}\right)\Delta\theta_{Ni^{3+}} + \left(\frac{\partial I_F}{\partial \theta_i}\right)\Delta\theta_i \quad (14)$$

The ratio $\Delta I_F/\Delta E$ is defined as the Faradaic admittance Y_F (inverse of the Faradaic impedance), thus

$$Y_F = \left(\frac{1}{R_t}\right) + \left(\frac{\partial I_F}{\partial \theta_{Ni^{3+}}}\right)\left(\frac{\Delta\theta_{Ni^{3+}}}{\Delta E}\right) + \left(\frac{\partial I_F}{\partial \theta_i}\right)\left(\frac{\Delta\theta_i}{\Delta E}\right) \quad (15)$$

R_t is the charge transfer resistance of the electrode reaction and its value is always positive.

Taking the linear approximation of Tailor's series expansion around the steady state, one has

$$jw\left(\frac{\Delta\theta_{Ni^{3+}}}{\Delta E}\right) = \left(\frac{\partial\dot{\theta}_{Ni^{3+}}}{\partial E}\right) + \left(\frac{\partial\dot{\theta}_{Ni^{3+}}}{\partial\theta_{Ni^{3+}}}\right)\left(\frac{\Delta\theta_{Ni^{3+}}}{\Delta E}\right) + \left(\frac{\partial\dot{\theta}_{Ni^{3+}}}{\partial\theta_i}\right)\left(\frac{\Delta\theta_i}{\Delta E}\right) \quad (16)$$

$$jw\left(\frac{\Delta\theta_i}{\Delta E}\right) = \left(\frac{\partial\dot{\theta}_i}{\partial E}\right) + \left(\frac{\partial\dot{\theta}_i}{\partial\theta_{Ni^{3+}}}\right)\left(\frac{\Delta\theta_{Ni^{3+}}}{\Delta E}\right) + \left(\frac{\partial\dot{\theta}_i}{\partial\theta_i}\right)\left(\frac{\Delta\theta_i}{\Delta E}\right) \quad (17)$$

and the Faradaic admittance can be written as

$$Y_F = \left(\frac{1}{R_t}\right) + \left(\frac{A}{B}\right) \quad (18)$$

Where

$$A = \left(\frac{\partial I_F}{\partial\theta_{Ni^{3+}}}\right)\left(\frac{\partial\dot{\theta}_{Ni^{3+}}}{\partial\theta_i}\right)\left(\frac{\partial\dot{\theta}_i}{\partial E}\right) + \left(\frac{\partial I_F}{\partial\theta_i}\right)\left(\frac{\partial\dot{\theta}_i}{\partial\theta_{Ni^{3+}}}\right)\left(\frac{\partial\dot{\theta}_{Ni^{3+}}}{\partial E}\right) - \left(\frac{\partial I_F}{\partial\theta_{Ni^{3+}}}\right)\left(\frac{\partial\dot{\theta}_i}{\partial\theta_i}\right)\left(\frac{\partial\dot{\theta}_{Ni^{3+}}}{\partial E}\right) - \left(\frac{\partial I_F}{\partial\theta_i}\right)\left(\frac{\partial\dot{\theta}_{Ni^{3+}}}{\partial\theta_{Ni^{3+}}}\right)\left(\frac{\partial\dot{\theta}_i}{\partial E}\right) + jw\left(\frac{\partial I_F}{\partial\theta_{Ni^{3+}}}\right)\left(\frac{\partial\dot{\theta}_{Ni^{3+}}}{\partial E}\right) + jw\left(\frac{\partial I_F}{\partial\theta_i}\right)\left(\frac{\partial\dot{\theta}_i}{\partial E}\right)$$

$$B = \left(\frac{\partial\dot{\theta}_{Ni^{3+}}}{\partial\theta_{Ni^{3+}}}\right)\left(\frac{\partial\dot{\theta}_i}{\partial\theta_i}\right) - \left(\frac{\partial\dot{\theta}_{Ni^{3+}}}{\partial\theta_i}\right)\left(\frac{\partial\dot{\theta}_i}{\partial\theta_{Ni^{3+}}}\right) - w^2 - jw\left(\frac{\partial\dot{\theta}_{Ni^{3+}}}{\partial\theta_{Ni^{3+}}}\right) - jw\left(\frac{\partial\dot{\theta}_i}{\partial\theta_i}\right)$$

In accordance with the above when $(\partial I_F/\partial\theta_i) > 0$ and $(\partial\dot{\theta}_i/\partial E) < 0$, positive resistance and when $(\partial I_F/\partial\theta_i) < 0$ and $(\partial\dot{\theta}_i/\partial E) > 0$

TABLE 1: Equivalent Circuit Parameters of Electrooxidation of 9 mM Glucose on GC/NiCu Electrode in NaOH Solution Obtained from Figure 7

E (V)	R_s (Ω)	R_1 (Ω)	$Q_1 \times 10^4$ (F)	$R_2 \times 10^{-2}$ (Ω)	$Q_2 \times 10^4$ (F)	$R_3 \times 10^{-2}$ (Ω)	$L \times 10^{-3}$ (H)	n_1	n_2
0.42	12	120	4	12.1	5.1			0.88	0.92
0.45	12.5	85	5	8	5.95			0.85	0.93
0.47	12.1	62	5.2	6.1	7			0.84	0.93
0.49	12.2	49	6.9	4.9	8.9	8	6.1	0.9	0.93
0.52	12	42	8	3.5	9.5	6.2	7.1	0.85	0.9
0.55	12	35	8.2	2.7	10.8	4.8	4.3	0.86	0.94
0.59	12.2	18	9	−2.5	10.9	1.7	0.7	0.87	0.96
0.62	11.9	12	10	−2	11	1.2	0.5	0.84	0.95
0.64	12.1	8	11.1	−1.6	12.9	0.9	0.3	0.88	0.92

TABLE 2: Values of Rate Constants Calculated from Equation 19 and Figure 7 for Electrooxidation of 9 mM Glucose on GC/NiCu Electrode in NaOH Solution

$k_1^o \times 10^{12}$ (mol cm^{-2}s^{-1})	$k_{-1}^o \times 10^5$ (mol cm^{-2}s^{-1})	$k_2 \times 10^8$ (mol cm^{-2}s^{-1})	$k_3 \times 10^7$ (mol cm^{-2}s^{-1})	$k_4^o \times 10^{10}$ (mol cm^{-2}s^{-1})	$k_5^o \times 10^6$ (mol cm^{-2}s^{-1})
4.9	2	4.1	2.5	3.5	1.6

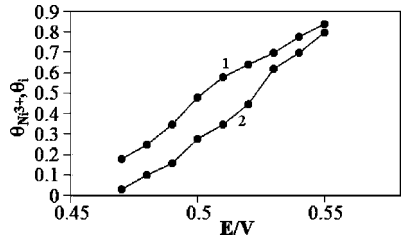

Figure 7. Calculated surface coverage of Ni^{3+} (1) and intermediates (2) for 9 mM glucose electrooxidation on GC/NiCu electrode.

negative resistance appears in the Nyquist diagrams. On the basis of reaction mechanism theoretical impedance was derived (eq 19) and the kinetic parameters are determined by fitting the model equation to the experimental Nyquist diagram (Table 2).

$$Y_F = \frac{1}{R_t} + \frac{a_9 a_4 + w a_{10} a_4 j + w^2 a_{10} a_{11} - a_9 w a_{11} j}{a_{12}} \quad (19)$$

$$c_1 = k_2\theta_{Ni^{3+}}C_g - k_3\theta_{Ni^{3+}}$$

$$a_1 = -k_2\theta_{Ni^{3+}}C_g - k_3\theta_{Ni^{3+}} - k_4C_g\theta_{Ni^{3+}} - k_5\theta_{Ni^{3+}}$$

$$a_2 = -2k_1 - 2k_{-1} + k_2C_g(1 - \theta_i) - k_3\theta_i$$

$$a_3 = k_2C_g(1 - \theta_i) - k_3\theta_i + k_4C_g(1 - \theta_i) - k_5\theta_i$$

$$a_4 = \frac{a_2F^2a_1}{q_1q_2} - \frac{c_1F^2a_3}{q_1q_2} - w^2$$

$$a_5 = \frac{k_4C_g\theta_{Ni^{3+}}(1 - \theta_i)}{b_4} - \frac{k_5\theta_{Ni^{3+}}\theta_i}{b_5}$$

$$a_6 = -k_4C_g\theta_{Ni^{3+}} + k_5\theta_{Ni^{3+}}$$

$$a_7 = \frac{2k_1(1 - \theta_{Ni^{3+}})}{b_1} - \frac{2k_{-1}\theta_{Ni^{3+}}}{b_{-1}}$$

$$a_8 = -2k_1 - 2k_{-1} + k_4C_g(1 - \theta_i) + k_5\theta_i$$

$$a_9 = \frac{a_8F^3c_1a_5}{q_1q_2} + \frac{a_6F^3a_3a_7}{q_1q_2} - \frac{a_8F^3a_1a_7}{q_1q_2} - \frac{a_6F^3a_2a_5}{q_1q_2}$$

$$a_{10} = \frac{a_8F^2a_7}{q_1} + \frac{a_6F^2a_5}{q_2}$$

$$a_{11} = -\frac{a_2F}{q_1} - \frac{a_1F}{q_2}$$

$$a_{12} = a_4^2 + w^2a_{11}^2$$

where q_1 and q_2 are charges required for complete Ni^{3+} formation or complete adsorption of intermediate on unit surface.

The corresponding coverage's of Ni^{3+} and the intermediates as a function of potential can be obtained from the model calculation and are presented in Figure 7. With the increase of potential, Ni^{3+} and the intermediates coverages rise. Also Ni^{3+} coverage approach unity in higher applied anodic potential.

So the impedance behaviors of glucose electrooxidation in different potential ranges can be categorized as follows:

(i) At low potential region (0.48 V), assuming reaction 5 is the rate-determining step and $\upsilon_5 < \upsilon_6$, then, $(\partial I_F/\partial\theta_i) > 0$, $(F/q_i)(\partial\upsilon_4/\partial E) - (\partial\upsilon_5/\partial E) < 0$, and the impedance diagram should show capacitive behavior with two overlapped capacitive semicircles appearing in the Nyquist plot and signifying a reaction with one adsorbed intermediate.[24] The EIS data are in line with the equivalent circuit presented in Figure 6a and reaction 5 seems to be the rate-determining step indeed.

(ii) At intermediate potential range (0.51 V), increasing the potential enhances the rate of reaction 5 but not enough to exceed that of reaction 6. In this case, the rate-determining step of glucose electrooxidation is in a transition region. In this case, $(\partial I_F/\partial\theta_i) < 0$, $(\partial\dot{\theta}_i/\partial E) < 0$, and it can be concluded that $(\partial I_F/\partial\theta_i)(\dot{\theta}_i/\partial E) > 0$.The inductive behavior observed in our experiments and shown in Figure 4b is predicted. The EIS data can be simulated using the equivalent circuit presented in Figure 6b. In this circuit R_1, R_2, Q_1, and Q_2 are the previously explained R_{ct}, R_{ads}, Q_{dl}, and Q_{ads} while R_3 is actually the inverse of the rate constant of the process of the regeneration of active sites for the adsorption and oxidation of glucose.In general, the condition of occurrence of an inductive behavior in the Nyquist plot is $(\partial I_F/\partial\theta_i)(\dot{\theta}_i/\partial E) > 0$. This implies that if the variation of the electrode potential causes a variation of the Faradaic current density not only through its effect on the strength of the electric field in the double layer but also through its effect on another variable and the both effects act in the same direction then an inductive component is expected in the impedance pattern.[47] According to impedance parameters $(\partial I_F/\partial\theta_i)$ and $(\partial\dot{\theta}_i/\partial E)$, inductive behavior in glucose electrooxidation reveals that the coverage's of the intermediates decreases with increasing potential and lead to an increase of Faradaic current. Apparently with increasing potential large amounts of Ni^{3+} are formed on the electrode surface and react with intermediates to decrease their coverage and also higher concentration of active site is available for reactions 5 and 6. Meanwhile, the decreasing surface coverage of intermediates will contribute to the adsorption of glucose on free sites which subsequently enhance the Faradaic current. So, at the intermediate potential range, with an increase of potential, the transition from capacitive behavior to inductive behavior indicates that the rate-determining step is changing.

(iii) At high potential range (0.54 V), reaction 6 can be assumed as a rate-determining step $k_5 \gg k_6$ and $\upsilon_5 > \upsilon_6$. In this case $(\partial I_F/\partial\theta_i) < 0$, $(\partial\dot{\theta}_i/\partial E) > 0$, and, thus, $(\partial I_F/\partial\theta_i)(\partial\dot{\theta}_i/\partial E) < 0$. The capacitive arc at the intermediate frequencies in the Nyquist plot will flips to the second quadrant with the real component of the impedance becoming negative. This means that passivation of electrode surface has occurred.[48] The EIS data can also be simulated using the equivalent circuit of Figure 6b. Melnick et al.[49] indicated that the passivation of the Pt electrode during methanol electrooxidation is probably due to the reversible formation of oxide species. Meanwhile, with reaction 6 being the rate-determining step the oxidation of intermediates with Ni^{3+} is much slower than the generation of intermediates by reaction 5 and the passivation at higher potentials can be explained by the formation of a large amount of intermediates on the surface of the catalyst. Therefore, adsorption of glucose is inhibited due to an increase of the coverage of intermediates and the electrooxidation rate shows almost no significant increase. As can be seen from the simulation of impedance plots with equivalent circuit (Table 1), it is observed that with the other elements remaining positive, the only parameter that will

cause the reversal of impedance pattern to the second, third and forth quadrants is R_2, the value of which is determined by electrode potential. At potentials lower than 0.53 V/Ag−AgCl R_2 decreases with the increase of applied anodic potential but in higher potential R_2 jumps to very negative values. Further increase of potential will lead to the decrease of absolute value of R_2. By comparing the potential dependence of simulated impedance pattern, it is found that, if R_2 is positive, the impedance will show the pattern similar to Figure 4a and b. If R_2 is negative, the reversing impedance pattern, as in Figure 4c, can be observed. The other element in equivalent circuit remains positive and decrease with increasing applied potential.

Assuming Fleischmann et al. mechanism for the electrooxidation on Ni electrode no negative resistance was obtained in the derivation of impedance equation. Therefore Fleischmann et al. mechanism does not fully accounts for the electrooxidation of glucose on Ni surface. The theoretical impedance diagrams obtained according to our proposed electrooxidation mechanism are in agreement with the negative resistance observed in the experimental impedance plots; therefore the proposed mechanism is a complete mechanism for the electrooxidation of glucose on GC/NiCu electrode.

4. Conclusion

The nickel oxide film was formed electrochemically on the previously electrodeposited nickel−copper alloy on a glassy carbon electrode in a regime of cyclic voltammetry and was tested for electrooxidation of glucose in alkaline media. Electrochemical impedance studies of glucose oxidation on GC/NiCu electrode demonstrate the potentialities of this method as a tool for investigating the mechanism of glucose oxidation. Different impedance patterns are observed for Ni and NiCu alloy electrode. Electrooxidation of glucose on GC/NiCu show negative resistance in impedance plots. The impedance data recorded at different potentials are analyzed and show evidence for two processes occurring at the interface: one is associated with the glucose electrooxidation leading to the intermediates formation on the surface and the other is assigned to the oxidation of intermediates. A theoretical impedance model based on kinetics is proposed which captures and explains all of the features of potential dependence of experimental impedance. The impedance behaviors in different potential regions reveal that the mechanism and rate-determining step in glucose electrooxidation vary with potential. At low potential region, glucose oxidation is rate-determining step, while at higher potentials, the oxidation and removal of adsorbed intermediates became rate-determining step. Meanwhile, at intermediate potential, the rate-determining step in glucose electrooxidation is in transition region. The theoretical impedance diagrams obtained according to our proposed electrooxidation mechanism are in agreement with the experimental impedance plots.

Acknowledgment. The authors wish to acknowledge the financial supports of the Office of Vice Chancellor of Research of their corresponding universities.

References and Notes

(1) Jin, C.; Chen, Z. *Synth. Met.* **2007**, *157*, 592.
(2) Kang, X.; Mai, Z.; Zou, X.; Cai, P.; Mo, J. *Anal. Biochem.* **2007**, *363*, 143.
(3) Katz, E.; Willner, I.; Kotlyar, A. B. *J. Electroanal. Chem.* **1999**, *479*, 64.
(4) Khoo, S. B.; Yap, M. G. S.; Huang, Y. L.; Guo, S. X. *Anal. Chim. Acta* **1997**, *351*, 133.
(5) Tominaga, M.; Shimazoe, T.; Nagashima, M.; Taniguchi, I. *J. Electroanal. Chem.* **2008**, *615*, 51.
(6) Nirmala Grace, A.; Pandian, K. *J. Phys. Chem. Solids* **2007**, *68*, 2278.
(7) Bagotzky, V. S.; Vassilyev, Y. B. *Electrochim. Acta* **1964**, *9*, 869.
(8) Bockris, JO'M.; Piersma, B. J.; Gileadi, E. *Electrochim. Acta* **1964**, *9*, 1329.
(9) Huang, W.; Zheng, J.; Li, Z. *J. Phys. Chem. C* **2007**, *111*, 16902.
(10) Morita, M.; Niwa, O.; Tou, S.; Watanabe, N. *J Chromatogr. A.* **1999**, *837*, 17.
(11) Wang, J.; Chen, G.; Chatrathi, M. P. *Electroanalysis* **2004**, *16*, 1603.
(12) Hilmi, A.; Luong, J. H. T. *Anal. Chem.* **2000**, *72*, 4677.
(13) Cheung, K.; Wong, W.; Ma, D.; Lai, T.; Wong, K. *Coord. Chem. Rev.* **2007**, *251*, 2367.
(14) Colon, L. A.; Dadoo, R.; Zare, R. N. *Anal. Chem.* **1993**, *65*, 476.
(15) Fleischmann, M.; Korinek, K.; Pletcher, D. *J. Chem. Soc., Perkin Trans.* **1972**, *2*, 1396.
(16) Luo, P.; Zhang, F.; Baldwin, R. P. *Anal. Chim. Acta* **1991**, *244*, 169.
(17) Zhao, J.; Wang, F.; Yu, J.; Hu, H. *Talanta* **2006**, *70*, 449.
(18) Miller, B. *J. Electrochem. Soc.* **1969**, *116*, 1675.
(19) Marioli, J.; Luo, P.; Kuwana, T. *Anal. Chim. Acta* **1993**, *282*, 571.
(20) Marioli, J.; Kuwana, T. *Electroanalysis* **1993**, *5*, 11.
(21) Boukamp, B. A. *Solid State Ion.* **1986**, *20*, 31.
(22) Harrington, D. A.; Conway, B. E. *Electrochim. Acta* **1987**, *32*, 1703.
(23) Amstrong, R. D. *J. Electroanal. Chem.* **1972**, *34*, 387.
(24) Amstrong, R. D.; Henderson, M. *J. Electroanal. Chem.* **1972**, *39*, 81.
(25) Seland, F.; Tunold, R.; Harrington, D. A. *Electrochim. Acta* **2006**, *51*, 3827.
(26) Muller, J. T.; Urban, P. M.; Holderich, W. F. *J. Power Sources* **1999**, *84*, 157.
(27) Chakraborty, D.; Chorkendorff, I.; Johannessen, T. *J. Power Sources* **2006**, *162*, 1010.
(28) van Hassel, B. A.; Boukamp, B. A.; Burggraaf, A. *J. Solid State Ion.* **1991**, *48*, 139.
(29) Orlik, M.; Jurczakowski, R. *J. Electroanal. Chem.* **2008**, *614*, 139.
(30) Gregori, J.; Garćia-Jareño, J. J.; Keddam, M.; Vicente, F. *Electrochim. Acta* **2007**, *52*, 7903.
(31) Macdonald, J. R. *Solid State Ion.* **1984**, *13*, 147.
(32) Jafarian, M.; Gobal, F.; Danaee, I.; Mahjani, M. G. *Electrochim. Acta* **2007**, *52*, 5437.
(33) Druska, P.; Strehblow, H. H.; Golledge, S. *Corros. Sci.* **1996**, *8*, 835.
(34) Bode, H.; Dehmelt, K.; Witte, J. *Electrochim. Acta* **1966**, *11*, 1079.
(35) Schrebler Guzman, R. S.; Vilche, J. R.; Arvia, A. J. *J. Electrochem. Soc.* **1978**, *125*, 1578.
(36) Chen, J.; Bradhurst, D. H.; Dou, S. X.; Liu, H. K. *J. Electrochem. Soc.* **1999**, *146*, 3606.
(37) Singh, D. J. *J. Electrochem. Soc.* **1998**, *145*, 116.
(38) Oshitani, M.; Watada, M.; Lida, T. In *Hydrogen and Metal Hydride Batteries*; Bennett, P. D., Sakai, T., Eds.; The Electrochemical Society Proceedings Series; The Electrochemical Society: Pennington, NJ, 1995; PV 94−27, p 303.
(39) Luo, P. F.; Kuwana, T.; Paul, D. K.; Sherwood, P. M. A. *Anal. Chem.* **1996**, *68*, 3330.
(40) Maritan, A.; Toigo, F. *Electrochim. Acta* **1990**, *35*, 141.
(41) Fleischmann, M.; Korinek, K.; Pletcher, D. *J. Electroanal. Chem.* **1971**, *31*, 39.
(42) Robertson, P. M. *J. Electroanal. Chem.* **1980**, *111*, 97.
(43) Vertes, G.; Horanyi, G. *J. Electroanal. Chem.* **1974**, *52*, 47.
(44) Taraszewska, J.; Roslonek, G. *J. Electroanal. Chem.* **1994**, *364*, 209.
(45) El-Shafei, A. A. *J. Electroanal. Chem.* **1999**, *471*, 89.
(46) Zhao, C.; Shao, C.; Li, M.; Jiao, K. *Talanta* **2007**, *71*, 1769.
(47) Cao, C. N. *Electrochim. Acta* **1990**, *35*, 831.
(48) Bagotzky, V. S.; Vassilyew, Y. B. *Electrochim. Acta* **1967**, *12*, 1323.
(49) Melnick, R. E.; Palmore, G. T. R. *J. Phys. Chem. B* **2001**, *105*, 9449.

JP8069173